The Formation and Stability of Adsorbed Formyl as a Possible Intermediate in Fischer−Tropsch Chemistry on Ruthenium

Gregg A. Morgan, Jr.,[†] Dan C. Sorescu,[†,‡] Tykhon Zubkov,[†] and John T. Yates, Jr.*,[†]

Surface Science Center, Department of Chemistry, University of Pittsburgh, Pittsburgh, Pennsylvania 15260, and U.S. Department of Energy, National Energy Technology Laboratory, Pittsburgh, Pennsylvania 15236

Density functional theory has been used to study the formation and stabilization of the chemisorbed formyl species, HCO, on the Ru(001) surface. It has been found that the η^1-HCO species attached to a Ru atom by a single Ru−C bond is unstable, and that it will convert to more strongly bound η^2- and η^3-HCO surface species. These more highly coordinated species decompose readily to produce H(a) and CO(a) via low activation energy reactions, indicating that the observation of HCO(a) species in any bonding mode at temperatures above 90 K is unlikely. Additionally, we found that abstraction of H from HCO(a) upon atomic H bombardment is another low-barrier reaction mechanism leading to the formation of adsorbed CO and desorption of an H$_2$ molecule. Using a stepped Ru(109) surface, containing atomic steps periodically located every 22 Å along the Ru(001) surface, we have bombarded chemisorbed CO with atomic H at $T < 170$ K in an attempt to produce and spectroscopically observe adsorbed HCO species by infrared reflection absorption spectroscopy. These experiments have been unsuccessful, and instead we have observed the surface crowding of CO(a) by H(a) species, and the displacement of CO(a) at high H(a) coverages. Both the experimental and theoretical results support the conclusion that the formyl species can be easily dissociated on the Ru surface. These studies throw into question previous measurements indicating that the interaction of atomic hydrogen with CO is effective in producing stable adsorbed formyl species on Ru.

I. Introduction

The hydrogenation of CO adsorbed on metal surfaces has been widely investigated due to its importance to the Fischer−Tropsch synthesis. Previous studies on the hydrogenation of CO utilized molecular hydrogen and were performed at pressures up to one atmosphere on both a clean Ru(001) substrate[1,2] as well as on a potassium-promoted Ru(001) surface.[3−5] Reaction products, as identified by vibrational spectroscopy, on the unpromoted surface include CH$_x$ and C−C species, whereas the K-promoted surface exhibited vibrational modes attributed to formyl as well as formate species.

Much work has been done on the coadsorption of CO and hydrogen in ultrahigh vacuum conditions on metal surfaces such as Pt,[6−8] Pd,[9] Ni,[7,10,11] Ru,[12−17] and Rh.[18] In all of these studies, it has been found that chemisorbed hydrogen, filling in the surface after CO adsorption, pushes the CO into immiscible islands in which the local coverage is elevated as a result of compression by the chemisorbed hydrogen. The first work, done on Rh(111),[18] showed that a p(2 × 2) CO structure was reversibly compressed into a $\sqrt{3} \times \sqrt{3}$ R 30° structure due to repulsive H...CO forces. Similar immiscibility between H(a) and CO(a) occurs on the Ru(001) surface.[14−16] No reaction is observed between H(a) and CO(a) under these conditions.[19]

Mitchell and Weinberg[20−22] reported that atomic H could drive chemisorbed CO to produce HCO(a) species at low temperatures on Ru(001). Their observations were made using high-resolution electron energy loss spectroscopy (HREELS).

Both formyl and formaldehyde surface species were reported to be formed. This reactivity observed was attributed to the high chemical potential of atomic H compared to 1/2 H$_2$(g).

We performed density functional calculations to examine the stability of the HCO(a) species in different bonding configurations, finding that decomposition to H(a) and CO(a) is likely to occur rapidly at the temperature of the experiments. Additionally, we found that abstraction of H from HCO(a) upon interaction with gas-phase atomic H, resulting in the formation of CO(a) and the desorption of H$_2$(g), is another possible HCO-(a) decomposition mechanism. We have also restudied the interaction of atomic H with CO(a) on the Ru(109) surface (which combines 22 Å wide Ru(001) terraces with stepped sites), finding that atomic H does not produce observable C−O or C−H infrared modes characteristic of chemisorbed HCO or H$_2$CO.

II. Theoretical Methods

The calculations performed in this study were done using the ab-initio total-energy VASP code.[23−25] This program evaluates the total energy of periodically repeating geometries based on density-functional theory and the pseudo potential approximation. In this case, only the valence electrons are represented explicitly in the calculations, the electron−ion interaction is described by fully nonlocal optimized ultrasoft pseudo potentials similar to those introduced by Vanderbilt[26] and provided by Kresse and Hafner.[27] Periodic boundary conditions are used with the occupied electronic orbitals expanded in a plane-wave basis. The expansion includes all plane waves whose kinetic energy $\hbar^2 k^2/2m < E_{cut}$ where k is the wave vector, m the electronic mass, and E_{cut} is the chosen

* Corresponding author.
† University of Pittsburgh.
‡ National Energy Technology Laboratory.

Fischer−Tropsch Chemistry on Ruthenium

J. Phys. Chem. B, Vol. 108, No. 11, 2004 **3615**

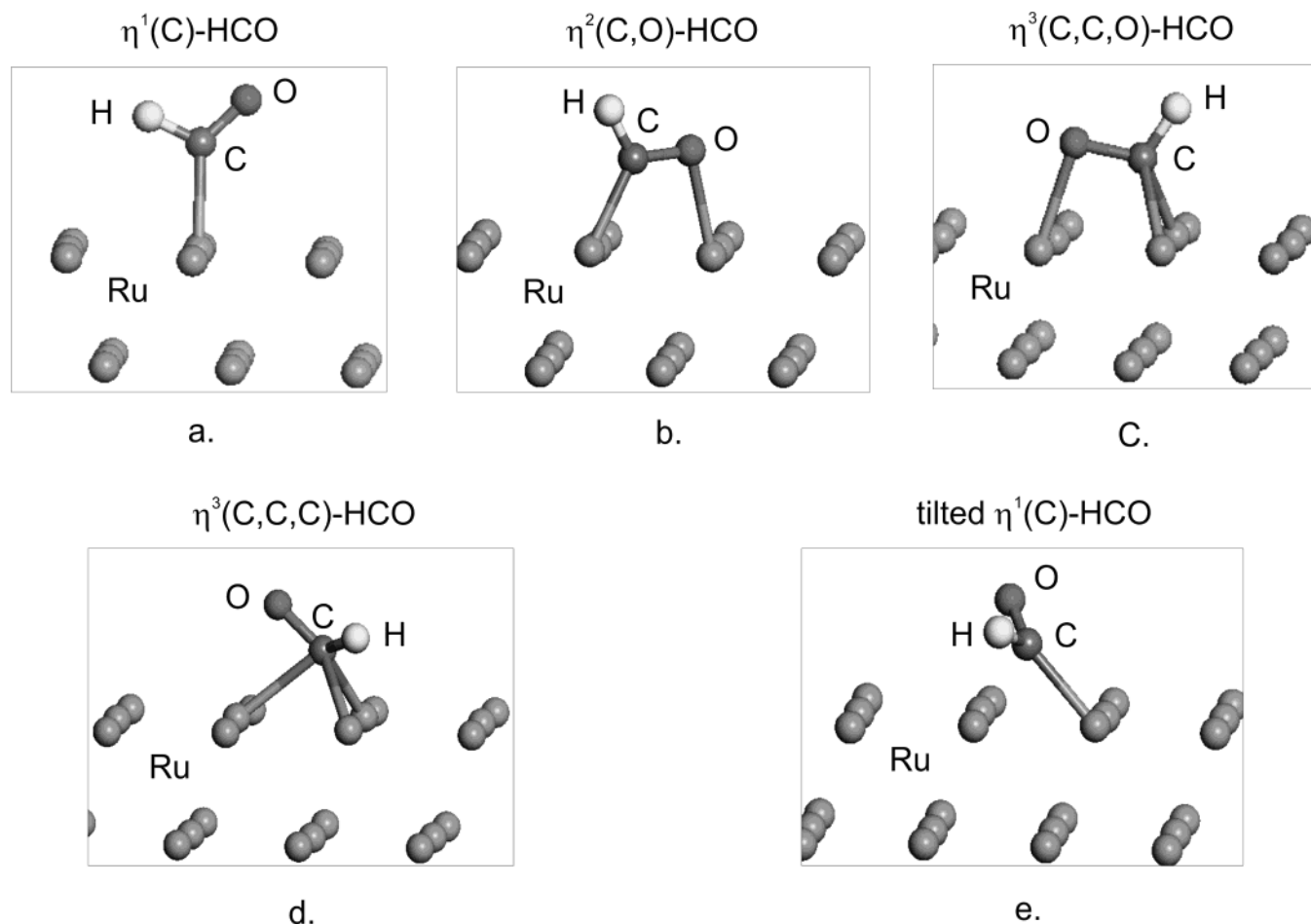## Various Adsorption Configurations of Formyl Species on Ru(001)

Figure 1. Pictorial view of the different adsorption configurations of the formyl radical on the Ru(001) surface considered in this study: (a) η^1(C)-HCO; (b) η^2(C,O)-HCO; (c) η^3(C,C,O)-HCO; (d) tilted η^3(C,C,C)-HCO; (e) tilted η^1(C)-HCO. Only the η^2(C,O)-HCO and η^3(C,C,O)-HCO have been identified as having a stable local minima. The other configurations correspond to saddle points on the potential surface.

cutoff energy. A cutoff energy of 396 eV has been employed in these studies. Electron smearing is employed via the Methfessel-Paxton technique[28] with a smearing width $\sigma = 0.2$ eV in order to minimize the errors in the Hellmann−Feynman forces due to the entropic contribution to the electronic free energy. All energies are extrapolated to $\sigma = 0$.

Calculations were performed using spin-polarized generalized gradient approximation (GGA) density functional theory using the PW91 exchange-correlation functional.[29] The minimization of the electronic free energy was performed using an efficient iterative matrix-diagonalization routine based on a sequential band-by-band residuum minimization method (RMM)[23,24] or alternatively based on preconditioned band-by-band conjugate-gradient (CG) minimization.[30] The optimization of different atomic configurations was performed based on a conjugate-gradient minimization of the total energy.

The surface model used in this study consists of a supercell with 3 × 3 surface units containing a four-layer slab. A vacuum width of about 10 Å has been chosen to separate neighbor slabs. The total number of Ru atoms in this model is 36. In calculations of molecular adsorption on the surface, we have relaxed all atomic positions of the molecule as well as the Ru atoms positioned in the first layer of the slab. The k-points sampling was generated on the basis of the Monkhorst-Pack scheme[31] with a 3 × 3 × 1 mesh. Minimum energy paths between

different minima were optimized by use of the nudged elastic band (NEB) method of Jónsson and co-workers.[32,33] In this approach, the reaction path is "discretized", with the discrete configurations, or images, between minima being connected by elastic springs to prevent the images from sliding to the minima in the optimization. Further checks of the convergence of the NEB calculations have been done by additional calculations in which the images corresponding to the transition state have been optimized using a quasi-Newton algorithm.

III. Theoretical Results

A. Methods Testing for Bulk Ru and Isolated HCO Molecule. Preliminary calculations to benchmark the accuracy of our DFT calculations have indicated that very good agreement is obtained for the prediction of bulk equilibrium crystallographic parameters. For example, from minimizations of the total energy of Ru(001) with respect to the volume of the unit cell within the experimentally determined $P6_3/mmc$ hexagonal space group symmetry, we have obtained the equilibrium lattice constants of $a = 2.729$ Å and $c = 4.318$ Å ($c/a = 1.5822$). These values are within 0.8% from the corresponding experimental numbers of $a_{\text{exp}} = 2.7058$ Å and $c_{\text{exp}} = 4.2816$ Å ($c_{\text{exp}}/a_{\text{exp}} = 1.5824$).[34]

An equally good representation has been observed for the geometric parameters of the isolated formyl radical. Based on

optimizations of the isolated formyl radical in a cubic box of $12 \times 12 \times 12$ Å^3, we have determined the following equilibrium bond lengths, $r(C-O) = 1.189$ Å, $r(C-H) = 1.128$ Å, and the bond angle $\theta(H-C-O) = 124.5°$. These values are in close agreement (within 1.1%) with the experimental values $r_{exp}(C-O) = 1.175$ Å, $r_{exp}(C-H) = 1.119$ Å, and $\theta_{exp}(H-C-O) = 124.4°$ reported by Hirota.[35] Consequently, the good agreement of our results for both bulk Ru and for isolated formyl molecular species made us confident to proceed to the next step, i.e. the investigation of molecular adsorption of HCO on the Ru(001) surface.

B. HCO Adsorption on Ru(001). The adsorption of the formyl radical on the Ru(001) surface has been examined for several different bonding configurations of this radical relative to the surface. For each configuration studied, the adsorption energy was determined according to the expression

$$E_{ads} = E_{molec} + E_{slab} - E_{(molec+slab)} \qquad (1)$$

where E_{molec} is the energy of the adsorbate species, E_{slab} is the total energy of the slab in the absence of the adsorbate, and $E_{(molec+slab)}$ is the total energy of the adsorbate/slab system. A positive E_{ads} corresponds to a stable adsorbate/slab system. The energy of the isolated adsorbate has been determined from calculations in a large simulation box of dimensions $12.0 \times 12.0 \times 12.0$ Å^3 and includes spin polarization corrections. The same Brillouin-zone sampling has been used to calculate the energies of the bare slab and of the adsorbate/slab systems.

Mitchell et al.[20-22] have suggested that exposing gas-phase atomic hydrogen to a saturated CO overlayer at 100 K on the Ru(001) surface will lead to formation of η^1- and η^2-formyl species similar to those depicted in Figure 1a and 1b. Upon annealing to 180 K, part of the η^1-formyl was reported to decompose to adsorbed CO and hydrogen, while the rest of η^1-formyl is converted to η^2-formyl. Following the previous experimental findings,[20-22] we considered first in our investigations the chemisorption properties of the formyl species in the vertical η^1 configuration (see Figure 1a). In this case the calculations have been done for the case of a single formyl molecule in the 3×3 surface supercell, corresponding to a coverage $\theta = 1/9$. On the basis of full optimizations of the formyl radical we have found that the η^1 adsorption configuration is not stable. Actually, during the optimization this configuration evolves toward the η^2 adsorption configuration depicted in Figure 1b. Despite starting the optimization procedure from several initial η^1-type configurations of formyl with different orientations and at different distances from the surface, we found that upon optimization all these lead to the η^2- or η^3-type (see below) adsorption configurations.

For the η^2 stable adsorption configuration, the C$-$O bond of formyl is almost parallel to the surface. Representative geometric and energetic parameters of this adsorption configuration denoted η^2(C,O)-HCO are given in Table 1. The "C,O" symbol used in the notation η^2(C,O)-HCO denotes the approximate bonding of the C and O atoms to the surface. We find that in this case the molecule binds to the surface through both C and O atoms at about $1.99-2.14$ Å from the Ru atoms. In this configuration the C$-$O bond is stretched by 0.086 Å relative to the gas-phase equilibrium distance in HCO. An overall binding energy of 59.6 kcal/mol has been determined for this adsorption configuration.

Another stable adsorption configuration of formyl we have determined is the η^3(C,C,O)-HCO horizontal configuration depicted in Figure 1c. In this case, the C atom binds in a bridge-

TABLE 1: The Calculated Geometric Parameters, Adsorption Energies, and Vibrational Frequencies for Formyl Species Adsorbed on the Ru(001) Surface[a]

Configuration	r(Ru-O)	r(Ru-C)	r(C-O)	r(C-H)	φ[b]	E_{ads}
HCO (gas phase, exp.)[c]			1.175	1.119	124.4	
HCO (gas phase, theo.)			1.188	1.129	124.5	
η^2(C,O)-HCO (theo.)	2.146	1.987	1.274	1.108	115.6	59.6
η^3(C,C,O)-HCO (theo.)	2.061	2.125	1.320	1.105	114.4	60.5
tilted η^3(C,C,C)-HCO (theo.)	...	2.055	1.264	1.317	112.5	
		2.186				
		2.142				
tilted η^1(C)-HCO (theo.)		2.045	1.262	1.254	112.3	

Configuration	ν_1 (C-H str)	ν_2 (C-O str)	ν_3(HCO-bend)
HCO (matix isolated, exp)[d]	2488	1860	1090
HCO (gas phase, exp.)[e]	2434	1868	1081
HCO (gas phase, theo.)	2625[f]	1861	1077
η^2(C,O)-HCO (theo.)	2911	1352	1210
η^3(C,C,O)-HCO (theo.)	2929	1142	1169
η^2(C,O)-HCO (exp)[g]	2900	1180	1400
η^2(C,O)-HCO (exp)[h]	2970	1190	1190

[a] All distances are in Å, adsorption energies are in kcal/mol, and frequencies are in cm^{-1}. [b] Angle between H$-$C$-$O, in degrees. [c] Data from ref 35. [d] Data from ref 53. [e] Data from ref 54 and references therein. [f] The calculated normal-mode frequency using VASP code in the harmonic approximation gives a value of 2625 cm^{-1}. However previous experimental[35,55] and theoretical[56] studies have indicated the existence of strong anharmonic effects and intermode coupling for the C$-$H stretching mode. When such effects are considered,[56] the calculated vibrational frequency decreases from 2815 to 2448 cm^{-1} in agreement with the experimental value of 2434$-$2488 cm^{-1}.[53,54] [g] Data from ref 41, referring to HCO(a) on Ru(001). [h] Data from ref 21, referring to HCO(a) on Ru(001).

type configuration to two-neighboring Ru atoms while the O atom is bonded to a single Ru atom. The binding energy of this configuration is slightly larger than that of the η^2(C,O)-HCO with a value of 60.5 kcal/mol. In this configuration, the CO bond is even more stretched by 0.132 Å relative to the isolated gas-phase equilibrium distance of HCO.

Finally, we present in panels (d) and (e) of Figure 1 two other configurations, the tilted η^3(C,C,C)-HCO and the tilted η^1(C)-HCO that were obtained by simple energy optimizations. Geometric parameters of these configurations are detailed in Table 1. However, further analyses of the potential energy surface (see the next paragraphs) have indicated that these configurations do not correspond to real equilibrium states but to saddle points.

Concluding this section we note that in the limit of low coverages where these calculations have been done we have identified two major adsorption configurations of the formyl radical denoted as η^2(C,O)-HCO and η^3(C,C,O)-HCO. The binding energies of these configurations are similar, in the range $59.6-60.5$ kcal/mol.

C. HCO Formation on Ru(001). Besides individual adsorption configurations of HCO on Ru(001) surface, a first problem we investigated was the minimum reaction path for the formation of adsorbed HCO upon interaction of gas-phase atomic H with an adsorbed CO molecule. These calculations have been done using the nudged elastic band method with eight images distributed along the reaction path and are presented in Figure 2. The initial configuration corresponds to H atom positioned at about 4.2 Å from the C atom of the CO molecule, while the final state represents HCO in a η^2(C,O) adsorption configuration. From these calculations it follows that the activation energy of this process is about 9 kcal/mol, indicating
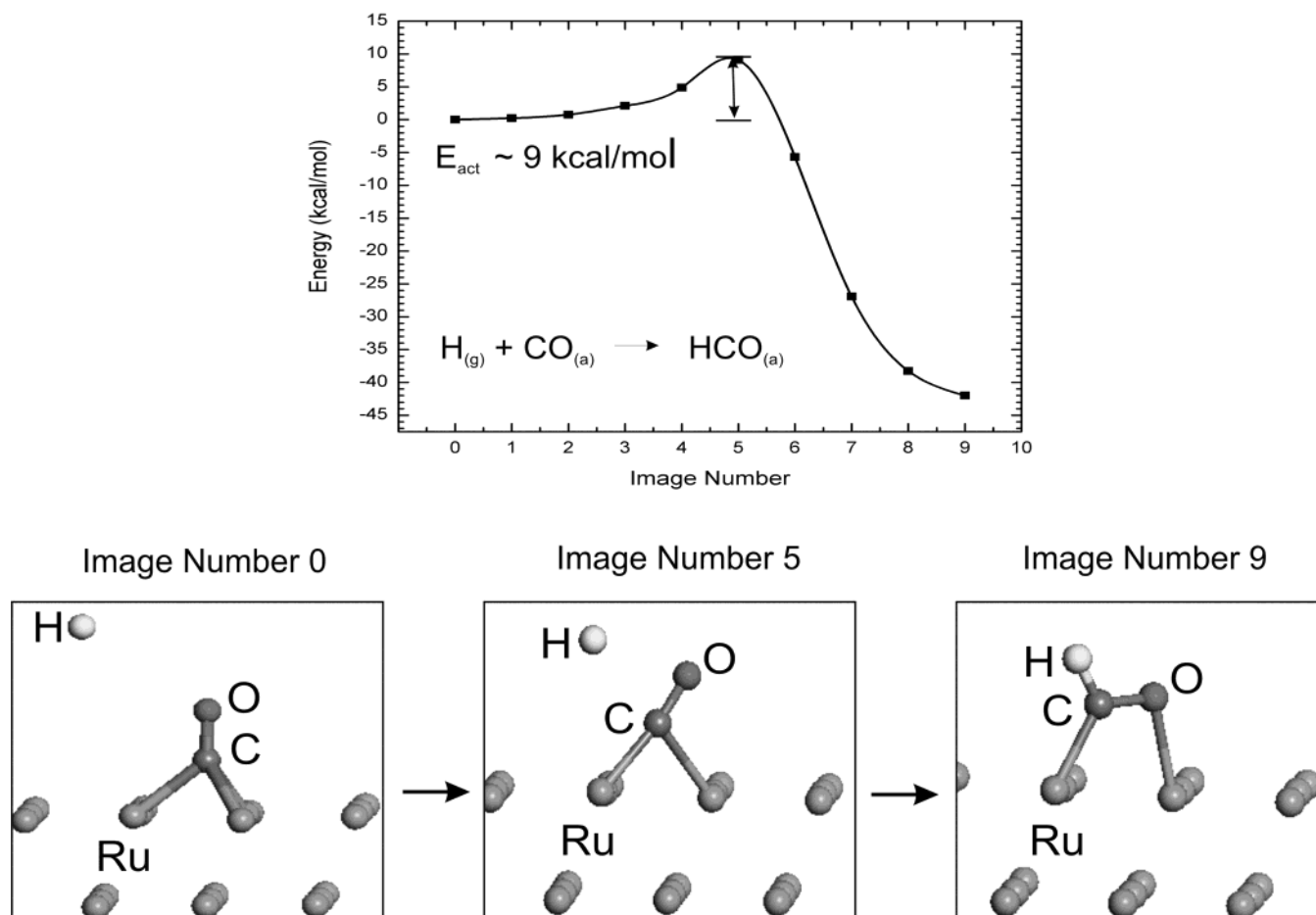
Formation of η^2(C,O)-HCO from CO(a) and H(g)

Figure 2. Potential energy surface for interaction of atomic H with adsorbed CO leading to formation of η^2(C,O)-HCO on the Ru(001) surface.

that HCO(a) can be readily be formed as a result of H bombardment of a CO molecule. However, we note that we have not attempted to map the angular distribution of the activation energy upon various incidence directions of the incoming atomic H. It is expected that higher activation energies might be required for more unfavorable attack directions of atomic H.

D. HCO Dissociation on Ru(001). A second problem we have analyzed theoretically is related to the energetic requirements for dissociation of the formyl species on the Ru(001) surface. We have analyzed the dissociation process for both η^2-(C,O)-HCO and η^3(C,C,O)-HCO adsorption configurations. These calculations have been done using the nudged elastic band method with eight images distributed along the reaction path. The corresponding minimum energy reaction pathways for dissociation of η^2 and η^3 formyl species are presented in Figures 3 and 4, respectively. We note that in both cases the activation energy for dissociation is relatively small with values of 7.4 kcal/mol for dissociation of η^2(C,O)-HCO and 4.1 kcal/mol for dissociation of η^3(C,C,O)-HCO. These results indicate that even if formyl species can be formed on the Ru(001) surface, these species will dissociate readily to CO and H. As a result, unless done at very low temperatures, measurements of vibrational bands should probe the stretching mode of CO adsorbed on the surface and not the CO stretching mode in the formyl radical.

Overall, the theoretical results presented in this section indicate that dissociation of formyl on the Ru(001) surface

leading to adsorbed CO and H takes place with relatively small activation energies between 4.1 and 7.4 kcal/mol, depending on the starting adsorption configuration.

E. Stability Investigations of the Tilted HCO Adsorption Configurations. We have further analyzed theoretically the potential energy surface for dissociation of formyl starting from the other configurations, i.e., tilted η^3(C,C,C)-HCO and tilted η^1(C)-HCO, identified in the optimization procedure and depicted in Figures 1d and 1e. Our calculations show that in both of these cases formyl dissociates to CO and H without an activation barrier. We present in Figure 5 only the corresponding potential energy path for dissociation of the tilted η^3(C,C,C)-HCO. As can be seen from this figure, the tilted η^3(C,C,C)-HCO configuration corresponds to a saddle point on the potential energy surface and does not represent a stable minimum.

F. Hydrogen Abstraction from Adsorbed HCO. A final process we have analyzed theoretically corresponds to the interaction of gas-phase atomic H with HCO adsorbed in a η^2-(C,O) configuration. Such a process is depicted in Figure 6. Initially, atomic H approaches the HCO molecule in a direction perpendicular to the surface, above the H atom of the HCO molecule. As a result of the interaction, the H atom of the HCO is abstracted leading to formation of H_2(g) and the adsorbed CO molecule. As illustrated in Figure 6, the activation energy for the abstraction process is quite small, indicating that such a reaction mechanism is likely even at low temperatures. This result further suggests that in practical experiments performed
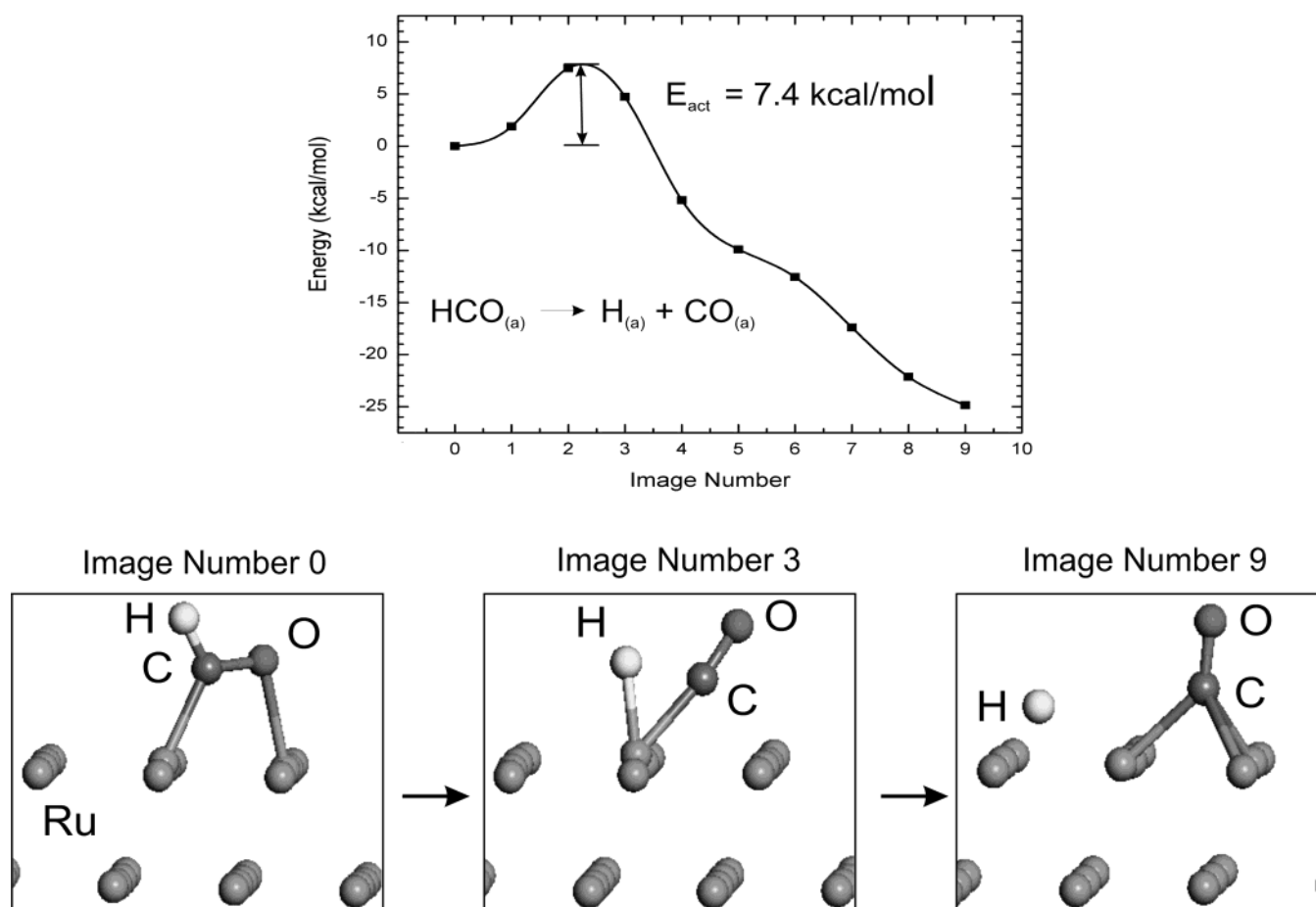
Dissociative Chemisorption of η^2(C,O)-HCO

Figure 3. Potential energy surface for dissociation of formyl to CO and H starting from the η^2(C,O)-HCO adsorption configuration.

at ordinary temperatures upon bombardment with atomic H, the concentration of HCO species on the surface will be low due to high reactivity with atomic H forming CO(a) and H$_2$(g). As in the case of the H(g) reaction with CO(a), we have not attempted to determine the angular dependence of the potential energy surface for different incident directions of atomic H upon adsorbed HCO. It is expected that the corresponding activation energies, even if they would have slightly larger values than those determined in the present case, will still indicate that abstraction of H from HCO is a readily possible mechanism.

G. Estimates of the Lifetime of Adsorbed HCO versus Temperature. If we assume a range of reasonable preexponential factors for adsorbed HCO decomposition, and use the activation energies calculated here, an estimate of the lifetime of the surface species can be made. We employ 170 K as the temperature, which is the highest temperature reached in our experiments to be described later. Thus, for the most stable η^2-(C,O)-HCO species, with an activation energy of dissociation of 7.4 kcal/mol, the half-life at 170 K ranges from 0.2 s to 2 × 10^{-5} s for preexponential factors from 10^{10} to 10^{14} s^{-1}. The next most stable η^3(C,C,O)HCO species, with an activation energy of dissociation of 4.1 kcal/mol, has a half-life at 170 K of only 10^{-5} to 10^{-9} s for the same range of preexponential factors. The η^1- HCO species is unstable, converting to η^2-HCO without appreciable activation energy. These estimates suggest that adsorbed HCO species in any bonding configuration would not be spectroscopically detectable at 170 K.

H. Calculated Vibrational Frequencies for Adsorbed HCO. The vibrational frequencies for the C−H stretching mode and for the C−O stretching mode of adsorbed HCO have been calculated. For the equilibrium adsorption configurations, η^2-(C,O)-HCO and η^3(C,C,O)-HCO, we have determined the corresponding vibrational frequencies (within the harmonic approximation) using a direct finite difference algorithm. The corresponding results are given in Table 1. As can be seen from these data, upon adsorption on the surface the CH stretch significantly increases from the gas-phase value (2434 cm^{-1}) to about 2911 cm^{-1} for η^2(C,O)-HCO and 2929 cm^{-1} for η^3-(C,C,O)-HCO. In contradistinction, the CO stretch decreases from the gas-phase value (1868 cm^{-1}) to 1352 cm^{-1} for η^2-(C,O)-HCO and to 1142 cm^{-1} for η^3(C,C,O)-HCO, suggesting a significant weakening of the C−O bond. These values are significantly smaller than the frequency of individual CO molecules adsorbed on the Ru(001) surface. For completeness we have also calculated the vibrational frequencies of CO when adsorbed at different surface sites, namely the on-top and hcp sites. Our results indicate that upon adsorption, CO vibrational frequency shifts from the calculated gas-phase value of 2096 cm^{-1} to 1950 cm^{-1} when adsorption takes place on-top or to 1700 cm^{-1} for an hcp adsorption site. As these values are well separated from those of CO in formyl, they should provide a practical procedure to separate C−O modes from HCO(a) and from chemisorbed CO.
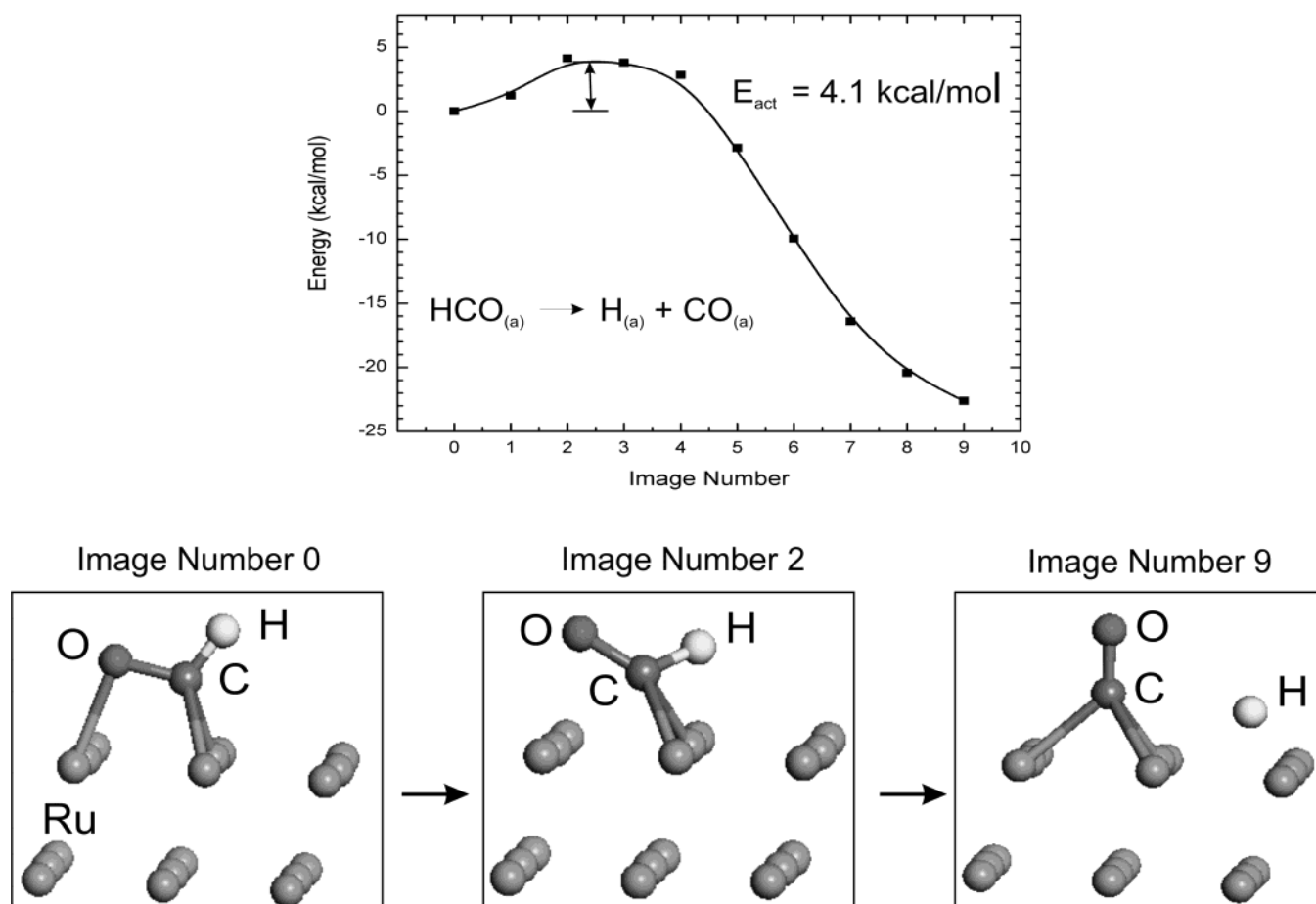
Fischer–Tropsch Chemistry on Ruthenium

J. Phys. Chem. B, Vol. 108, No. 11, 2004 **3619**

Dissociative Chemisorption of η^3(C,C,O)-HCO

Figure 4. Potential energy surface for dissociation of formyl to CO and H starting from the η^3(C,C,O)-HCO adsorption configuration.

IV. Experimental Methods

All of the experiments reported here were performed in a stainless steel ultrahigh vacuum (UHV) chamber with a base pressure below 1.0×10^{-10} mbar. The apparatus was equipped with a quadrupole mass spectrometer (QMS), an Auger Electron Spectrometer (CMA), a 4-grid LEED apparatus using a hemispherical phosphor screen, a Fourier-transform infrared reflection absorption (FT-IRAS) spectrometer, an absolutely calibrated capillary array molecular beam doser, an ion extractor pressure gauge, as well as a variable flow leak valve for system dosing.

The sample was a Ru(109) single crystal prepared by *ESCETE Single-Crystal Technology B.V.* The crystal was oriented 11.46° from the ⟨001⟩ direction toward the ⟨100⟩ direction. The Ru(109) surface is composed of periodic close-packed (001) terraces of 10 atomic row width (22 Å) separated by double height atom steps of ⟨101⟩ orientation. Characterization of the single crystal was achieved by means of low-energy electron diffraction (LEED), and the results are reported in detail elsewhere.[36] The crystal was spot welded to two 1.0 mm diameter W wires for efficient heating and cooling. A base temperature of ~88 K may be obtained with liquid N_2 cooling, and maximum heating to 1700 K is obtained with resistive heating assisted by electron bombardment on the backside of the crystal by means of a tungsten coil. The temperature of the crystal was measured with a W–Re (5–26% Re) thermocouple spot welded to the backside of the crystal.

The sample was cleaned initially by extended Ar^+ ion sputtering (~12–13 h), which was then followed by a series of sputtering and annealing procedures using an oxygen beam at 1200 K. The crystal was then subjected to additional oxygen treatment in which it was exposed to the oxygen beam (effective pressure in the beam ~5×10^{-8} mbar) as the temperature was cycled between 1123 and 1200 K. Following each oxygen treatment, the adsorbed layer of oxygen was removed by annealing the crystal to 1700 K briefly. After 15 cycles of oxygen treatment, the sample exhibited a clean Auger spectrum.[36] One such cycle of the O_2 cleaning was used for daily cleaning of the crystal.

The infrared reflection–absorption spectra were obtained by means of a Mattson-Cygnus FTIR spectrometer upgraded to model 4236. The double-beam optical bench is described in detail elsewhere.[37] The infrared radiation was p-polarized with respect to the surface of the crystal, and spectra were collected using 4 cm^{-1} resolution averaged over 2000 scans.

$^{12}C^{16}O_{(g)}$ (AGA, 99.999% purity) was dosed onto the surface of the crystal via the molecular beam doser.[38,39] The molecular beam doser allowed for absolute exposure control as well as minimization of the background pressure rise. The intercepted fraction of the beam by the crystal was found to be ~20% for our crystal-doser geometry, determined experimentally by the adsorption of low vapor pressure compounds such as HCHO, CH_3CHO, and $(CH_3)_2CO$, which have an initial sticking

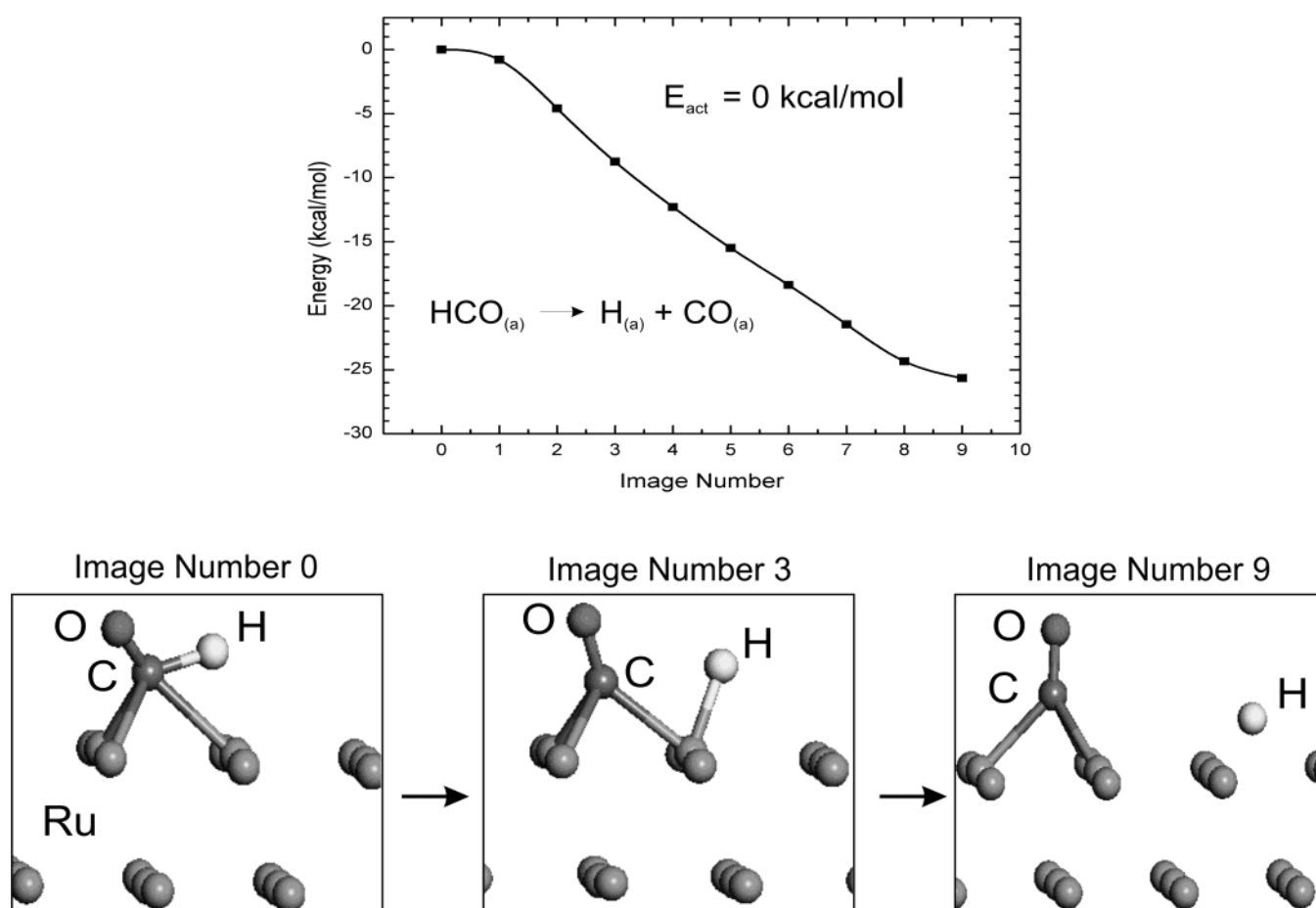## Dissociative Chemisorption of Tilted η^3(C,C,C)-HCO

Figure 5. Potential energy surface for dissociation of formyl to CO and H starting from the tilted η^3(C,C,C)-HCO configuration.

coefficient very close to unity on Ru at 88 K forming condensed multilayers as the coverage is increased. The correlation between $^{12}C^{16}O_{(g)}$ exposure and coverage has been determined previously and the results are reported by Zubkov et al.[36] Following any exposure to CO, the crystal was heated to 250 K and cooled immediately to 88 K. This procedure was designed to equilibrate and order the CO adlayer without depletion as no CO desorbs from the surface at this temperature.[40] Atomic hydrogen was generated by dissociating $^1H_2$ (Valley National Gases, 99.9995% purity) with a hot tungsten coil (approximately 1800 K as measured by an optical pyrometer). The measured brightness temperature of the tungsten coil was corrected for the emissivity of tungsten as well as for absorption by the window. The hydrogen was admitted into the chamber by means of the variable flow leak valve in order to back-fill the chamber. The ion gauge was used to measure the pressure in the chamber and the readings were corrected for gauge sensitivity, using a relative sensitivity factor of 0.6 for hydrogen. The crystal was positioned about one centimeter in front of the W-coil with the (109) face directed toward the W-coil. During the atomization of the hydrogen, the temperature of the crystal rose from 88 K to approximately 150 K, for a 50 s exposure. For a 100-s exposure, the temperature rose to approximately 170 K. Following each exposure to atomic hydrogen, the sample was linearly heated to 150 K to desorb any water, which may have been generated by H atoms striking the chamber walls.[22] All hydrogen exposures are reported in Langmuirs (1 L = 1 × 10⁻⁶

Torr s) and represent the molecular hydrogen exposure. The efficiency of the atomization of the molecular hydrogen, and therefore the actual atomic hydrogen exposure, is not known. The crystal was biased at −100 V during the hydrogen exposure so as to avoid thermionically generated electrons from the W-coil from reaching the crystal.

V. Experimental Results

$^{12}C^{16}O$ was initially adsorbed on the surface up to a saturation coverage which corresponds to 7.47 × 10¹⁴ cm⁻², ($\theta_{CO} = 0.54$ relative to the available ruthenium surface atoms). An infrared spectrum of the saturated adlayer was recorded and is plotted in Figure 7a. A single infrared band at 2064 cm⁻¹ is the only observable feature. This frequency corresponds to the C−O stretching frequency of on-top CO species and is consistent with our previous results.[40] The saturated surface was then exposed to 1250 L of H/H₂. The resulting infrared spectrum is plotted in Figure 7b. A single infrared band at 2052 cm⁻¹ was the only observable feature. The peak intensity of this feature was approximately 1/4 of the peak intensity of the infrared band of the saturated surface. The integrated band absorbance corresponding to the pure CO layer is approximately 5 times larger than the band corresponding to the CO layer treated with atomic H. In addition to a decrease in the intensity and hence the area of the absorbance peak there is also a significant broadening of the infrared band. The infrared band of the pure CO on the surface has an initial full width at half-maximum (fwhm) of
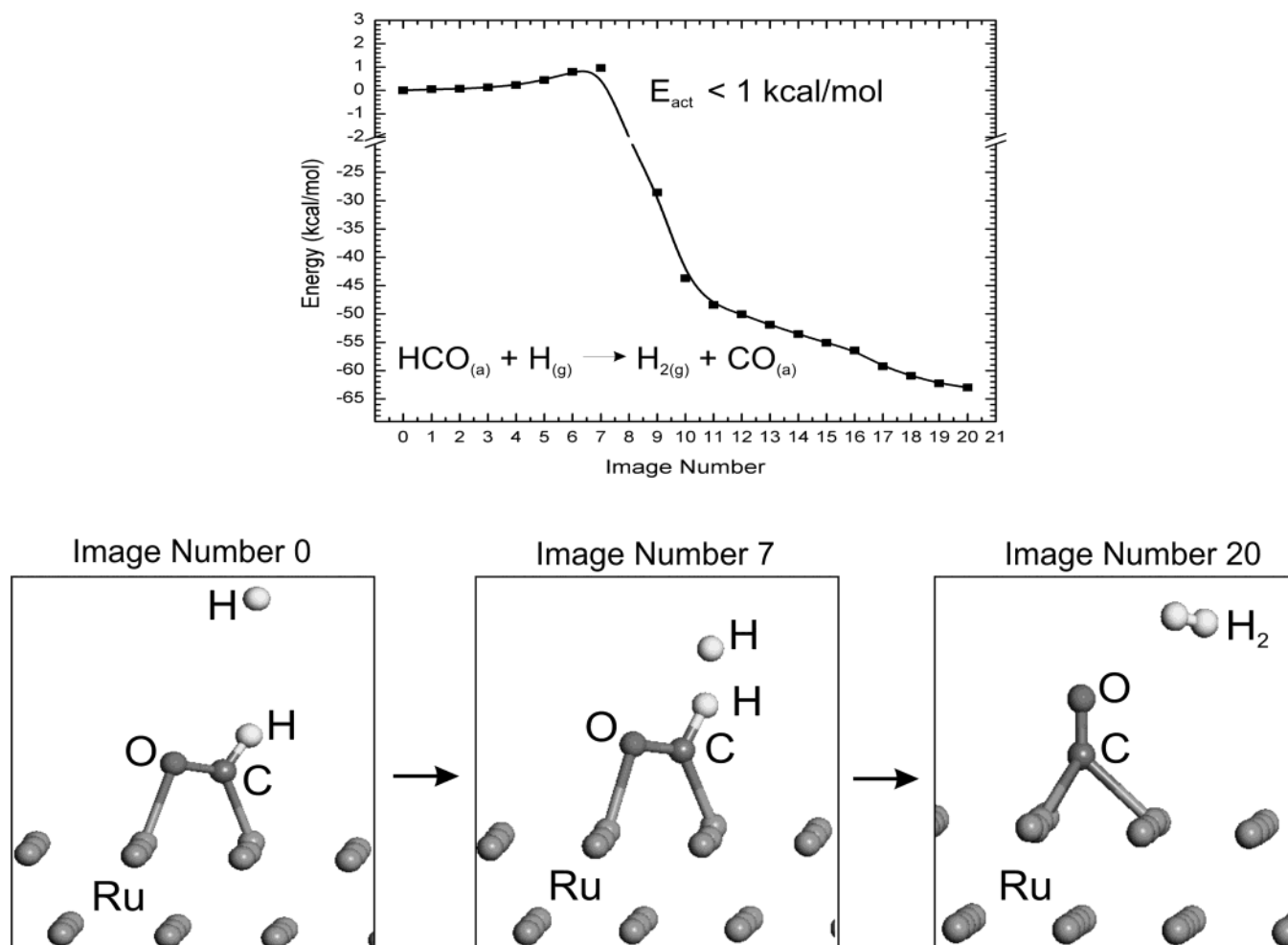
Fischer−Tropsch Chemistry on Ruthenium

J. Phys. Chem. B, Vol. 108, No. 11, 2004 **3621**

Hydrogen Abstraction from η^2(C,O)-HCO

Figure 6. Potential energy surface for H abstraction from η^2(C,O)-HCO with the formation of adsorbed CO and desorption of an H_2 molecule.

approximately 9 cm^{-1}, whereas the infrared band after the H/H$_2$ exposure has a fwhm of about 22 cm^{-1}. This increase in the CO line width may be attributed to the increased inhomogeneity of the CO adlayer as the CO adlayer is initially ordered in Figure 7a. The broad scan spectrum in Figure 7b shows that no other infrared features in the range of 3500 cm^{-1} to 800 cm^{-1}, expected for a chemical reaction between atomic H and chemisorbed CO, are observed after extensive atomic H exposure. The sensitivity of the measurements is < 0.0006 A units.

In a separate experiment ^{12}C^{16}O was adsorbed on the surface to a coverage of 5.51 × 10^{14} cm^{-2} (θ_{CO} = 0.40 relative to the available ruthenium surface atoms), approximately 74% of the saturation coverage. The behavior of the CO adlayer following various H/H$_2$ exposures was followed by infrared spectroscopy. The initial infrared spectrum of the pure CO adlayer produced a single band at 2038 cm^{-1}. The CO adlayer was then exposed to increasing exposures of atomic hydrogen from 6 to 1250 L H/H$_2$, with a spectrum being recorded after each exposure. After an initial exposure of 6 L of H/H$_2$ the infrared frequency shifted rapidly upward to 2055 cm^{-1}. The CO band continues to increase in frequency as the cumulative hydrogen exposure increases, reaching a maximum frequency of 2061.5 cm^{-1} after an exposure of 19 L of H/H$_2$. As the cumulative H/H$_2$ exposure continues to increase, the infrared band then shifts downward

in frequency and gradually loses intensity. After an exposure of 1250 L of H/H$_2$ the frequency of the band is 2045 cm^{-1} as can be seen in Figure 8. Again no other development of absorbances over the frequency range 3500 cm^{-1} to 800 cm^{-1} is observed. A control experiment was performed in order to verify that the atomic hydrogen (and not spurious effects from the walls of the chamber) was in fact responsible for the observed effect on the CO adlayer. In this control experiment, ^{12}C^{16}O was adsorbed on the surface at the same coverage as in the previous experiment (θ_{CO} = 0.40 relative to the available ruthenium surface atoms), but the backside of the crystal (instead of the front side (109 face) as previously) was directed toward the W-coil during the generation of atomic hydrogen. In this experiment, the single infrared band shifted from an initial frequency of 2038 cm^{-1} upward to 2054 cm^{-1} (data not shown) while gradually losing intensity and becoming broader as the exposure of H/H$_2$ increases to its maximum value of 1250 L.

The changes in the CO-frequency are plotted against the hydrogen exposure in Figure 9. In a control experiment, the same coverage of CO was adsorbed onto the surface of the Ru-(109) crystal, but instead of being exposed to atomic hydrogen, the adlayer was only exposed to molecular hydrogen and the results are plotted in Figure 9. There is a very gradual increase in the CO frequency, from 2035 cm^{-1}, as the exposure of molecular hydrogen is increased. The slight difference in the

Effect of Large Atomic H Exposure
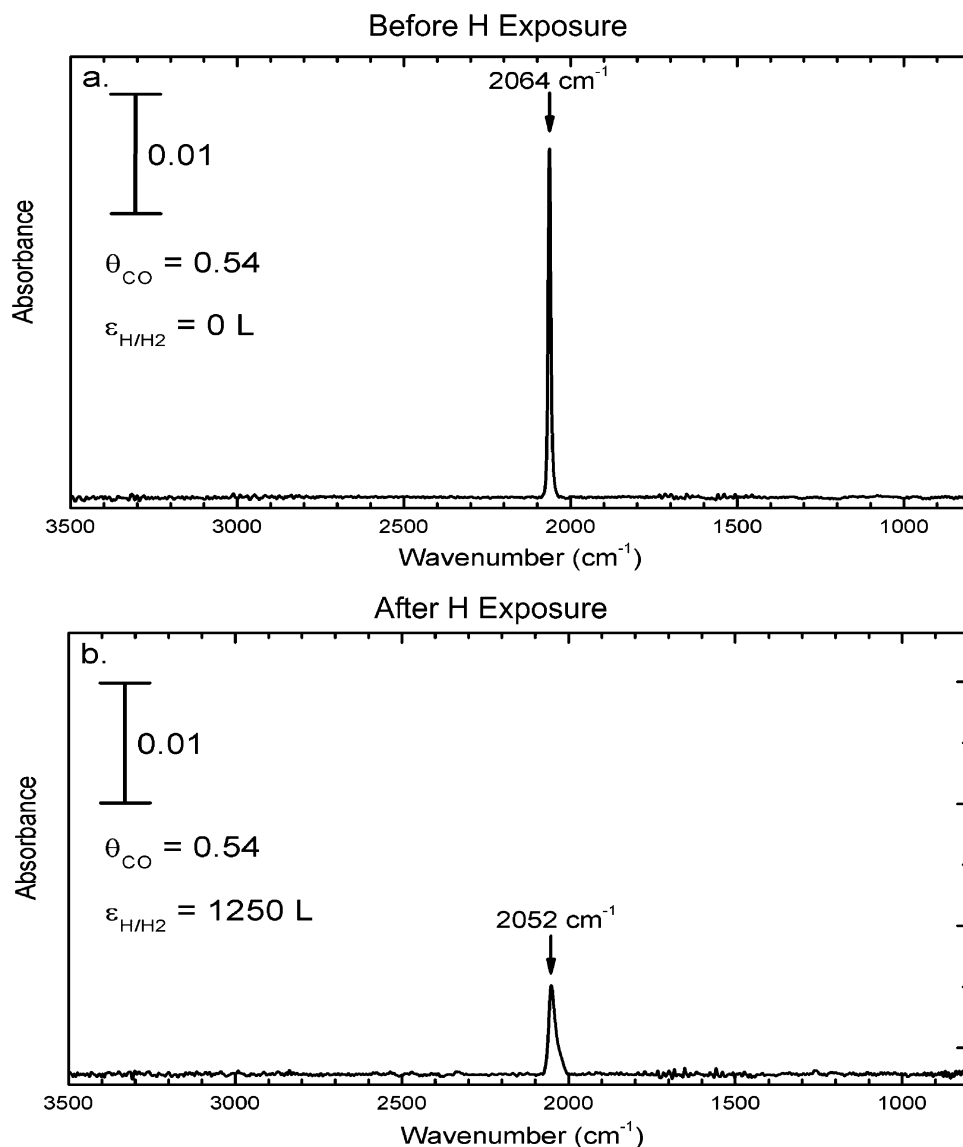# on CO/Ru(109) at Full Coverage

Figure 7. Infrared spectra of chemisorbed CO on Ru(109), $\theta_{CO} = 0.54$. (a) Prior to atomic hydrogen exposure; and (b) after 1250 L of atomic hydrogen exposure.

initial frequencies can be attributed to a slight difference in the initial coverage of CO adsorbed on the surface. After an H_2 exposure of 1250 L, the CO frequency shifted upward, by 11 cm^{-1}, to 2046 cm^{-1}. This comparison between H/H$_2$ and H$_2$ exposures shows that most of the effect with the H/H$_2$ mixture is due to the presence of atomic H in the incident gas mixture. It is likely that supplying hydrogen at high chemical potential (compared to H$_2$) causes rapid H coadsorption with CO.

VI. Discussion

A. The Production of HCO(a) from Atomic H and CO on Ru. The theoretical investigations of the adsorbed HCO species on Ru(001) indicate that at 150 K, the temperature employed in this work, if these species were produced they would not be observable by vibrational spectroscopy. Work by Anton et al.[41] and by Mitchell et al.[20-22] has reported the presence of stable η^1-HCO at 100 K and the conversion of this species to η^2-HCO at 180 K, as well as its decomposition. The

production of adsorbed H$_2$CO is also reported.[20-22] These results are in disagreement with our theoretical estimates of the stability of η^2-HCO, and also with our reflection infrared measurements, where neither C−H modes nor C−O modes of HCO(a) were observed.

It is possible that the explanation of our experimental results is connected with the stringent normal-dipole selection rule for infrared reflection spectroscopy,[42] a limiting rule less strongly applicable to HREELS.[43,44] As shown in Figure 1a, the η^1-HCO species presents a C−O and a C−H bond which each possess a large normal component, and η^1-HCO should therefore be observable by IR reflection spectroscopy, if it is thermally stable. However, the η^2-HCO species does not have a large normal component for the C−O stretching mode, although the C−H stretching mode should be visible by reflection IR.

Previous studies involving transmission IR spectroscopy on Al$_2$O$_3$-supported Rh catalysts have been carried out in a search for the production of adsorbed HCO by reaction of chemisorbed
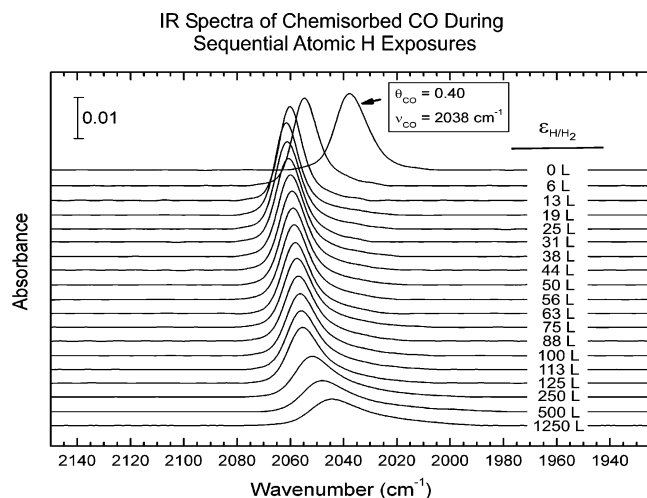
Fischer−Tropsch Chemistry on Ruthenium

J. Phys. Chem. B, Vol. 108, No. 11, 2004 **3623**

Figure 8. Infrared spectra of chemisorbed CO on Ru(109) at an initial coverage of $\theta_{CO} = 0.40$, after sequential atomic hydrogen exposures. The hydrogen gas was admitted to the chamber through a variable flow leak valve and was atomized by means of a tungsten coil at approximately 1800 K. The temperature of the crystal rose to about 150 K during the exposures. The crystal was biased −100 V during the exposures.

CO with atomic H at 170 K.[45] These experiments, which are not limited by the dipole selection rule, were also completely negative. The use of a high-surface-area metallic catalyst adds extra sensitivity to the infrared measurements.

B. Shifts in the C−O Stretching Mode Following Exposure of Chemisorbed CO to Atomic H: CO Compression and Displacement Effects. It is well-known that when the coverage of CO is increased on Ru(001), the CO frequency shifts upward.[46] This effect has also been seen on Ru(109).[36] The upward shift is due to interaction between the dynamic dipoles of the CO oscillators, in which the in-phase coupling, leading to a higher mode frequency, is preferentially intensified compared to out-of-phase coupling[42] as the coverage is increased.

When hydrogen coadsorbs with chemisorbed CO, immiscible islands of H(a) and CO(a) are formed, causing the local coverage in the CO islands to increase. The upward frequency shift initially observed in the C−O mode (Figure 6) when either atomic H or H_2 interacts with the surface containing CO is therefore likely to be due to this CO compression effect. The same effect is seen with D atoms interacting with chemisorbed CO on Ru(001).[12] The higher chemical potential of atomic H causes this coadsorption process to be kinetically accelerated compared to experiments employing H_2. An alternate explanation[12,17] involving an electronic interaction between H(a) and CO(a) is unlikely to be strongly involved.

After an exposure to H/H_2 of only about 20 L, the increase in C−O frequency is reversed, and ν_{CO} begins to decrease. This is likely due to the displacement of chemisorbed CO by atomic H. The reduction in C−O frequency at higher atomic H exposures is accompanied by a large loss in C−O band intensity, also suggesting that CO displacement by atomic H has occurred. The extra potential energy of atomic H compared to H_2 [1/2 D_0 (H_2) = 52.1 kcal/mol] may kinetically drive CO displacement. At $\theta_{CO} = 0.40$, we have measured that the binding energy of CO is only about 15 kcal/mol.[36] The exothermicity of atomic H adsorption is 58−65 kcal/mol,[47] based on the desorption activation energy of H_2 (11−26 kcal/mol of H_2).[48]

C. HCO as an Intermediate in Fischer−Tropsch Chemistry. These experiments do not address the possibility that chemisorbed HCO intermediates may be involved in the Fischer−Tropsch catalytic reaction. If HCO is an intermediate in the reaction, its steady-state surface concentration will be very low at ordinary synthesis temperatures. For high-pressure H_2, where pressure is employed to elevate the chemical potential, it is likely that CO displacement processes will occur under catalytic conditions. Many other studies suggest that the alternative kinetic route to Fischer−Tropsch alkane products involving C−O bond scission is active.[49−52]

VII. Summary

Theoretical investigations suggest that at temperatures of 170 K, formyl species adsorbed on Ru(001) will be unstable, and
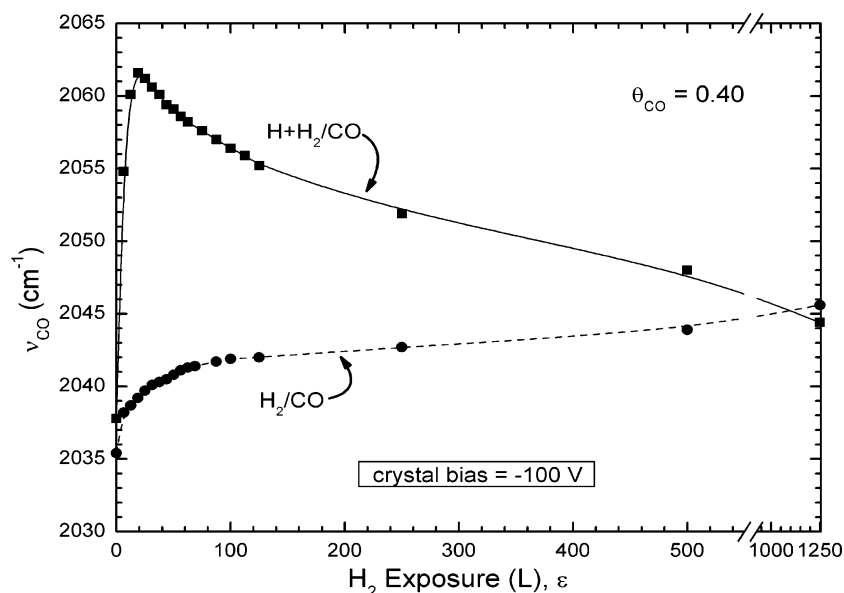

Figure 9. Comparison of infrared spectra of chemisorbed CO on Ru(109) at an initial coverage of $\theta_{CO} = 0.40$, after sequential exposures of atomic and molecular hydrogen. The crystal was biased −100 V during the exposures.

will rapidly decompose to H(a) and CO(a). HCO species multiply bound in different ways on Ru via C and O moieties exhibit low dissociation activation energies of only 7.4−4.1 kcal/mol and are unstable at $T >$ 170 K. Additionally, our theoretical results suggest that H atom-induced H abstraction from formyl species with formation of CO(a) and desorption of $H_2(g)$ is another possible reaction mechanism at low temperatures.

Using reflection IR spectroscopy, a search for HCO species produced by atomic H bombardment of chemisorbed CO has not revealed the production of these species, consistent with theoretical expectations on Ru.

Atomic H is observed to cause CO overlayer compression effects, based upon observations of an initial increase in C−O vibrational frequency as immiscible H(a) and CO(a) islands are produced. Continued exposure to atomic H causes desorption of CO at 150−170 K as deduced by a downward shift in the C−O frequency as well as a large decrease in integrated CO IR absorbance.

References and Notes

(1) Sakakini, B.; Steeples, B.; Dunhill, N.; Vickerman, J. C. *Stud. Surf. Sci. Catal.* **1989**, *48*, 817.
(2) Wu, M. C.; Goodman, D. W.; Zajac, G. W. *Catal. Lett.* **1994**, *24*, 23.
(3) Hoffmann, F. M.; Weisel, M. D. *Surf. Sci.* **1991**, *253*, L402.
(4) Weisel, M. D.; Chen, J. G.; Hoffmann, F. M. *J. Electron Spectrosc. Relat. Phenom.* **1990**, *54−55*, 787.
(5) Weisel, M. D.; Robbins, J. L.; Hoffmann, F. M. *J. Phys. Chem.* **1993**, *97*, 9441.
(6) Henderson, M. A.; Yates, J. T., Jr. *Surf. Sci.* **1992**, *268*, 189.
(7) Peebles, D. E.; Creighton, J. R.; Belton, D. N.; White, J. M. *J. Catal.* **1983**, *80*, 482.
(8) Wang, H.; Tobin, R. G.; Lambert, D. K.; Fisher, G. B.; DiMaggio, C. L. *Surf. Sci.* **1995**, *330*, 173.
(9) Kiskinova, M.; Bliznakov, G. *Surf. Sci.* **1982**, *123*, 61.
(10) Bauhofer, J.; Hock, M.; Küppers, J. *J. Electron Spectrosc. Relat. Phenom.* **1987**, *44*, 55.
(11) White, J. M. *J. Phys. Chem.* **1983**, *87*, 915.
(12) Braun, J.; Kostov, K. L.; Witte, G.; Wöll, C. *J. Chem. Phys.* **1997**, *106*, 8262.
(13) Jakob, P.; Gsell, M.; Menzel, D. *J. Chem. Phys.* **2001**, *114*, 10075.
(14) Mak, C. H.; Deckert, A. A.; George, S. M. *J. Chem. Phys.* **1988**, *89*, 5242.
(15) Peebles, D. E.; Schreifels, J. A.; White, J. M. *Surf. Sci.* **1982**, *116*, 117.
(16) Riedmüller, B.; Papageorgopoulos, D. C.; Berenbak, B.; van Santen, R. A.; Kleyn, A. W. *Surf. Sci.* **2002**, *515*, 323.
(17) Wang, R. L. C.; Kreuzer, H. J.; Jakob, P.; Menzel, D. *J. Chem. Phys.* **1999**, *111*, 2115.
(18) Williams, E. D.; Thiel, P. A.; Weinberg, W. H.; Yates, J. T., Jr. *J. Chem. Phys.* **1980**, *72*, 3496.
(19) Weinberg, W. H. *Acc. Chem. Res.* **1996**, *29*, 479.
(20) Mitchell, W. J.; Wang, Y.; Xie, J.; Weinberg, W. H. *J. Am. Chem. Soc.* **1993**, *115*, 4381.
(21) Mitchell, W. J.; Xie, J.; Jachimowski, T. A.; Weinberg, W. H. *J. Am. Chem. Soc.* **1995**, *117*, 2606.
(22) Mitchell, W. J.; Xie, J.; Wang, Y.; Weinberg, W. H. *J. Electron Spectrosc. Relat. Phenom.* **1993**, *64−65*, 427.
(23) Kresse, G.; Furthmüller, J. *Phys. Rev. B: Condens. Matter* **1996**, *54*, 11169.
(24) Kresse, G.; Furthmüller, J. *Comput. Mater. Sci.* **1996**, *6*, 15.
(25) Kresse, G.; Hafner, J. *Phys. Rev. B: Condens. Matter* **1993**, *48*, 13115.
(26) Vanderbilt, D. *Phys. Rev. B: Condens. Matter* **1990**, *41*, 7892.
(27) Kresse, G.; Hafner, J. *J. Phys.: Condens. Matter* **1994**, *6*, 8245.
(28) Methfessel, M.; Paxton, A. T. *Phys. Rev. B: Condens. Matter* **1989**, *40*, 3616.
(29) Perdew, J. P.; Chevary, J. A.; Vosko, S. H.; Jackson, K. A.; Pederson, M. R.; Singh, D. J.; Fiolhais, C. *Phys. Rev. B: Condens. Matter* **1992**, *46*, 6671.
(30) Kresse, G.; Hafner, J. *Phys. Rev. B: Condens. Matter* **1993**, *47*, 558.
(31) Monkhorst, H. J.; Pack, J. D. *Phys. Rev. B: Condens. Matter* **1976**, *13*, 5188.
(32) *Classical Quantum Dynamics in Condensed Phase Simulations*; Berne, B. J.; Ciccotti, G.; Coker, D. F., Eds.; World Scientific: Singapore, 1998.
(33) Mills, G.; Jónsson, H.; Schenter, G. K. *Surf. Sci.* **1995**, *324*, 305.
(34) *CRC Handbook of Chemistry and Physics*; 81st ed.; Linde, D. R., Ed.; Boca Raton, FL, 2001.
(35) Hirota, E. *J. Mol. Struct.* **1986**, *146*, 237.
(36) Zubkov, T.; Morgan, G. A., Jr.; Yates, J. T., Jr.; Kühlert, O.; Lisowski, M.; Schillinger, R.; Fick, D.; Jänsch, H. J. *Surf. Sci.* **2003**, *526*, 57.
(37) Xu, Z.; Yates, J. T., Jr. *J. Vac. Sci. Technol., A* **1990**, *8*, 3666.
(38) Winkler, A.; Yates, J. T., Jr. *J. Vac. Sci. Technol., A* **1988**, *6*, 2929.
(39) Yates, J. T., Jr. *Experimental Innovations in Surface Science*; AIP Press: Springer-Verlag: New York, 1998.
(40) Zubkov, T.; Morgan, G. A., Jr.; Yates, J. T., Jr. *Chem. Phys. Lett.* **2002**, *362*, 181.
(41) Anton, A. B.; Parmeter, J. E.; Weinberg, W. H. *J. Am. Chem. Soc.* **1986**, *108*, 1823.
(42) Hoffmann, F. M. *Surf. Sci. Rep.* **1983**, *3*, 107.
(43) Ibach, H.; Mills, D. L. *Electron Energy Loss Spectroscopy and Surface Vibrations*; Academic Press: New York, 1982.
(44) Kolasinski, K. W. *Surface Science: Foundations of Catalysis and Nanoscience*; John Wiley and Sons Ltd.: West Sussex, 2002.
(45) Yates, J. T., Jr.; Cavanagh, R. R. *J. Catal.* **1982**, *74*, 97.
(46) Pfnür, H.; Menzel, D.; Hoffmann, F. M.; Ortega, A.; Bradshaw, A. M. *Surf. Sci.* **1980**, *93*, 431.
(47) Capitano, A. T.; Gabelnick, A. M.; Gland, J. L. *Surf. Sci.* **1999**, *419*, 104.
(48) Schwarz, J. A. *Surf. Sci.* **1979**, *87*, 525.
(49) Adesina, A. A. *Appl. Catal., A: General* **1996**, *138*, 345.
(50) Anderson, R. B. *The Fischer−Tropsch Synthesis*; Academic Press: New York, 1984.
(51) Rofer-DePoorter, C. K. *Chem. Rev.* **1981**, *81*, 447.
(52) Storch, H. H.; Golumbic, N.; Anderson, R. B. *The Fischer−Tropsch and Related Syntheses*; John Wiley & Sons: Chapman & Hall: New York, London, 1951.
(53) Milligan, D. E.; Jacox, M. E. *J. Chem. Phys.* **1964**, *41*, 3032.
(54) Dane, C. B.; Lander, D. R.; Curl, R. F.; Tittel, F. K.; Guo, Y.; Ochsner, M. I. F.; Moore, C. B. *J. Chem. Phys.* **1988**, *88*, 2121.
(55) Milligan, D. E.; Jacox, M. E. *J. Chem. Phys.* **1969**, *51*, 277.
(56) Bowman, J. M.; Bittman, J. S.; Harding, L. B. *J. Chem. Phys.* **1986**, *85*, 911.